Biochimica et Biophysica Acta 1828 (2013) 1025–1035

Contents lists available at SciVerse ScienceDirect

Biochimica et Biophysica Acta

journal homepage: www.elsevier.com/locate/bbamem

Growth kinetics of lipid-based nanodiscs to unilamellar vesicles—A time-resolved small angle neutron scattering (SANS) study

Suanne Mahabir [a], Darcy Small [b], Ming Li [c], Wankei Wan [a,b,*], Norbert Kučerka [d], Kenneth Littrell [e], John Katsaras [d,e,f], Mu-Ping Nieh [c,*]

[a] Biomedical Engineering Graduate Program, The University of Western Ontario, London, Ontario, Canada, N6A 5B9
[b] Department of Chemical and Biochemical Engineering, The University of Western Ontario, London, Ontario, Canada, N6A 5B9
[c] Institute of Materials Science, Chemical Materials & Biomolecular Engineering Department, University of Connecticut, Storrs, CT 06269, USA
[d] National Research Council, Canadian Neutron Beam Centre, Chalk River, Ontario, Canada
[e] Neutron Sciences Directorate, Oak Ridge National Laboratory, Oak Ridge, TN 37831, USA
[f] Joint Institute for Neutron Sciences, Oak Ridge National Laboratory, Oak Ridge, TN 37831, USA

ARTICLE INFO

Article history:
Received 7 June 2012
Received in revised form 1 November 2012
Accepted 2 November 2012
Available online 26 November 2012

Keywords:
Nanodisc
Low temperature annealing
Unilamellar vesicle
Spontaneous formation
Self-assemble
Reaction limited coalescence

ABSTRACT

Mixtures of dimyristoyl-phosphatidylcholine (DMPC), dimyristoyl-phosphatidylglycerol (DMPG) and dihexanoyl-phosphatidylcholine (DHPC) in aqueous solutions spontaneously form monodisperse, bilayered nanodiscs (also known as "bicelles") at or below the melting transition temperature of DMPC (T_M ~23 °C). In dilute systems above the main transition temperature T_M of DMPC, bicelles coalesce (increasing their diameter) and eventually self-fold into unilamellar vesicles (ULVs). Time-resolved small angle neutron scattering was used to study the growth kinetics of nanodiscs below and equal to T_M over a period of hours as a function of temperature at two lipid concentrations in presence or absence of NaCl salt. Bicelles seem to undergo a sudden initial growth phase with increased temperature, which is then followed by a slower reaction-limited growth phase that depends on ionic strength, lipid concentration and temperature. The bicelle interaction energy was derived from the colloidal theory of Derjaguin and Landau, and Verwey and Overbeek (DLVO). While the calculated total energy between discs is attractive and proportional to their growth rate, a more detailed mechanism is proposed to describe the mechanism of disc coalescence. After annealing at low temperature (low-*T*), samples were heated to 50 °C in order to promote the formation of ULVs. Although the low-*T* annealing of samples has only a marginal effect on the mean size of end-state ULVs, it does affect their polydispersity, which increases with increased *T*, presumably driven by the entropy of the system.

Published by Elsevier B.V.

1. Introduction

The structure of bilayered discoidal micelles—also known as "bicelles"—has been proposed in aqueous solutions containing mixtures of long-chain [e.g., dimyristoyl-phosphatidylcholine (DMPC), dimyristoyl-phosphatidylglycerol (DMPG)] and short-chain (or detergent-like) [e.g., dihexanoyl-phosphatidylcholine (DHPC)] lipids. Bicelles, for example, have been extensively used as magnetically alignable substrates (at temperatures between 30 and 50 °C) for elucidating the structure of membrane-associated proteins by nuclear magnetic resonance (NMR) spectroscopy [1–6]. Initially, these nano-sized discs (nanodiscs) were thought to make up the magnetically alignable morphology. However, subsequent small angle neutron scattering (SANS) [7,8] and cryogenic transmission electron microscopy [9,10] experiments determined that the magnetically alignable morphology was most likely composed of perforated lamellae or interconnected, elongated bilayered ribbons. Nevertheless—as determined by SANS—nanodiscs do exist at low temperature (<20 °C), wherein the planar disc region is mostly composed of long-chain gel lipids and the high-curvature disc rim is occupied by short-chain L_α lipids (or detergents) [3-5, 11-18]. Although nanodiscs are not magnetically alignable, their importance is no less than that of the perforated lamellae, since they are the precursors to nano-sized, low-polydispersity, self-assembled unilamellar vesicles (ULVs), which can serve as delivery vehicles for therapeutics and as imaging probes [12,19].

Several theoretical models have been proposed regarding the formation of ULVs from planar membranes, many of which are based on the system's curvature energy. It was determined that the membrane's charge density can affect its bending rigidity, elastic modulus of Gaussian curvature and its spontaneous curvature, leading to the formation of ULVs [20]. Some studies also have indicated that the introduction of a charged lipid can induce perforations and defects in the lipid bilayer [21]. With the exception of a few studies, most models describe the ULV bilayer as a uniform membrane, where the molecular inhomogeneity of the bilayer's inner and outer leaflets is not taken into consideration [22,23].

The transformation of nanodiscs into ULVs as a function of increasing temperature has been proposed to take place in three stages:

* Corresponding authors. Tel.: +1 860 486 8708; fax: +1 860 486 4745.
E-mail address: mu-ping.nieh@ims.uconn.edu (M.-P. Nieh).

0005-2736/$ – see front matter. Published by Elsevier B.V.
http://dx.doi.org/10.1016/j.bbamem.2012.11.002

(1) nanodiscs grow in size by coalescing with each other; (2) at some point, nanodiscs become unstable because of insufficient amounts of the short-chain lipid or detergent covering the nanodisc's rim; and (3) the enlarged nanodiscs fold onto themselves forming stable ULVs [10,12,18,19]. The nanodisc-to-ULV transition as a function of increasing temperature is triggered by the migration of short-chain lipids from the disc's rim to its planar region (due to increased miscibility with the long-chain lipids) [24], causing the rim line tension to increase, which then drives the nanodiscs to coalesce and eventually to self-fold into ULVs in order to reduce the possibility of exposing hydrocarbon chains to water. The proposed model has been corroborated by a series of SANS studies that looked at the effect of charge density, salinity and thermal path on the end-state ULV morphology [25]. However, it was also found that self-assembled ULVs could be obtained, even at low temperatures (i.e., far below the melting transition temperature of the long-chain lipid, T_M), suggesting that the growth and self-folding processes of nanodiscs could take place when the long-chain (DMPC) and short-chain (DHPC) lipids are in different phases (i.e., gel and L_α, respectively). A recent study also showed that bilayered ribbons formed prior to ULV formation in weakly charged systems (high-salinity systems), and that the time for such a transformation was on the order of hours [26]. These latest observations suggest that nanodiscs, although they form consistently, may not be thermodynamically stable. Here we are interested in addressing the following questions: 1) what conditions dictate nanodisc growth, and at a given temperature do they grow up to a certain size prior to transforming into ULVs; and 2) how does the rate of disc growth depend on lipid concentration, charge density, salinity and temperature? An understanding of these two issues will enable us to better control the self-assembling process of this system.

In order to gain insight into the low temperature (below T_M) growth of nanodiscs, and its effect on ULV morphology above T_M, time-resolved SANS studies were performed using a phospholipid mixture composed of DMPC, DHPC and DMPG. The growth of nanodiscs was investigated as a function of temperature, on samples of two lipid concentrations in the presence and absence of salt. Nanodisc growth after dilution at $T<T_M$ was observed and can partially be described by the Derjaguin and Landau, and the Verwey and Overbeek (DLVO) theory [27,28]. ULV terminal size is correlated with the size of the nanodiscs from which they were formed, giving an indication of the nanodisc aggregation number. The data show that the terminal ULV size strongly depends on lipid concentration, but is practically independent of the final size of the nanodiscs that were annealed at different T_{anneal}.

2. Material and methods

2.1. Sample preparation

Lipids (i.e., DMPC, DMPG, DHPC) were purchased from Avanti Polar Lipids (Alabaster, AL) and used without further purification. Samples of a fixed molar ratio ([DMPC]/[DMPG]/[DHPC] = 50/0.5/15) were prepared in D_2O and two NaCl concentrations (i.e., [NaCl] = 0 mM and 3 mM), at an initial total lipid concentration (C_{lp}) of 20 wt.% following a previously reported procedure [19], and were stored at 4 °C. The molar ratio of lipids is chosen based on the previous studies where the nanodisc-to-vesicle transformation formed robustly [11,12,19,25,26]. Prior to SANS experiments, the 20 wt.% samples were diluted to a C_{lp} of 1 and 0.3 wt.% at 4 °C using the corresponding buffers (0 or 3 mM) and stored at 4 °C for ~10 h. Subsequent to this, the samples were transferred to the sample stage of the SANS instrument, which was pre-equilibrated at each annealing temperature, T_{anneal} (= 10, 17 and 23 °C), at which point data collection was initiated. The sample temperature should increase to the preset T_{anneal} immediately because of the small sample amount (<0.5 mL), It should be noted that the first SANS data set was obtained *10–20 min* after a change in temperature (i.e., from 4 °C to 10, 17 or 23 °C). As a result, the growth of nanodiscs in the first 20 min of each T_{anneal} (i.e., 10, 17 or 23 °C is not reported).

SANS data were then collected at each T as a function of "annealing" time over 10–15 min of intervals. The final step involved heating each sample to 50 °C (conducted in a preheated oven) for >4 h. The end-state ULVs at 50 °C were also characterized by SANS.

2.2. SANS

SANS experiments were performed using the CG-2 SANS instrument, which is located at ORNL (Oak Ridge National Lab, Oak Ridge, TN). An incident neutron beam with a wavelength (λ) of 4.75 Å, two sample-to-detector distances (4 and 18.5 m), and a detector offset of 20 cm were used to cover a range of scattering vectors, $q\left[=\frac{4\pi}{\lambda}\sin\left(\frac{\theta}{2}\right)\right.$, where θ is the scattering angle] from 0.0035 $Å^{-1}$ to 0.35 $Å^{-1}$. All two-dimensional data were circularly averaged with respect to the beam center to yield a one-dimensional intensity profile, which was then put on an absolute scale (cross section per unit volume) using a standard procedure. The resultant intensity, $I(q)$ as a function of q can be written as follows:

$$I(q)\sim\phi\left\langle |F(q)|^2 S(q)\right\rangle + I_{inc}, \quad (1)$$

where ϕ is the volume fraction of the aggregates; $F(q)$ is the form factor amplitude; $S(q)$ is the structure factor which describes the inter-particle interaction between the aggregates in solutions; I_{inc} is the incoherent scattering which was determined from the plateau of the scattering data at high q, and which was then subtracted from the individual reduced data sets. Raw data were corrected for sample transmission, ambient background (blocked beam), and empty cell scattering (signal from an empty sample cell) and then put on the absolute scale using the known scattering cross-section of a silica standard. The neutron data collected at the two sample-to-detector distances were then spliced together. Data corrections were conducted using the data reduction program (in IGOR-Pro) developed at NIST (National Institute of Standards and Technology) Center for Neutron Research [29]. Hayter and Penfold [30,31] described an analytical expression for $S(q)$ by solving the Ornstein–Zernike equation with the mean spherical approximation. This method accounts for the electrostatic repulsive interactions between charged particles, and is determined using the total lipid concentration, the solvent's dielectric constant, the surface charge density of the lipid bodies, and the ionic strength of the solution. $S(q)$ was used when fitting the data from charged ULVs and nanodiscs, with the exception of the very dilute and [NaCl]-doped systems, where $S(q)$ is assumed to be unity, and is therefore not required. However, it should be noted that the Hayter–Penfold $S(q)$ is derived based on spherical geometry. For discoidal or vesicular aggregates, the true volume occupied by the aggregates and the real Coulombic interactions are normalized and simplified. As a result, the average charge numbers of the aggregates may not be accurate. However, the model was capable of capturing the main feature of the particular interactions.

The amplitude of the form factor, $F(q)$ was determined using the *Core Shell Disk* (CSD) and *Polydisperse Vesicle* (PV) models for bicelles and ULVs, respectively [29]. A detailed description of both models can be found in the supporting information or references elsewhere [7,26]. The CSD model describes the lipid bilayer as having an outer hydrophilic region, representing the lipid head groups, and an inner hydrophobic region, representing the acyl chains, which are sandwiched between the hydrophilic regions. The bilayer thickness was determined to be 50 ± 5 Å, consistent with previous reports [32]. During the fitting procedure, the scattering length densities of D_2O ($\rho_{solvent}$), the hydrophobic core ($\rho_{hydrophobic}$) and the hydrophilic shell ($\rho_{hydrophilic}$) were constrained to the calculated and literature values $\times 10^{-6}$ $Å^{-2}$, -4.3×10^{-7} $Å^{-2}$ and 3.3×10^{-6} $Å^{-2}$, respectively [11,33]. The core radius and the shell thickness were obtained from the best fits to the data.

The PV model describes a spherical shell made up of a single bilayer, wherein a constant neutron scattering length density is assumed for the lipid bilayer ($\rho_{bilayer} = 3.2\times10^{-7}$ Å^{-2}). This is justified on the basis that there is a sharp contrast (i.e., interface) between the D_2O and the lipid, such that the sharp interface between these two features is well-described by a square well distribution. The shell thickness was constrained between 25 and 35 Å. The ULV inner radius was assumed to follow a Schulz distribution with a polydispersity, p defined as the ratio of standard deviation, σ to the average vesicle radius, R_v (i.e., $p = \sigma/R_v$). Both R_v and p were obtained from the best fits to the data.

2.3. Zeta potential

Within 30 min of sample preparation the Zeta potential, ζ was measured using a Malvern Zetasizer 3000HSA. The zeta potential was measured in triplicate, and the averages of the results were used for modeling purposes.

3. Results and discussion

3.1. Bicelle growth

The effects of ionic strength ([NaCl] = 0, 3 mM), total lipid concentration (C_{lp} = 0.3, 1 wt.%) and temperature (T = 10, 17 and 23 °C) on the growth of bicelles was investigated using SANS. As shown in Fig. 1, the SANS results illustrate three general patterns, all of which point to the presence of nanodiscs. For small, non-interacting nanodiscs (e.g., 1 wt.% [NaCl] = 3 mM sample at T_{anneal} = 10 and 17 °C) the SANS curve contains a low-q plateau region, followed by a gradual transition from q^{-2} to q^{-4} (slope of the data), and finally the incoherent background. For interacting nanodiscs (e.g., 1 wt.% [NaCl] = 0 mM), an extra broad peak due to the structure factor $S(q)$ is observed at q<0.02 Å^{-1}. The S(q) results from the high charge density on the particles and is described by the Hayter-Penfold model (in Material and methods section). The best-fit parameters from this model are revealed in supporting information. The third SANS pattern is characterized by a continuous q^{-2} dependence replacing the low-q plateau region, suggesting the presence of a large planar aggregates, most likely large discs (e.g., [NaCl] = 3 mM, 23 °C). As a result, the best fit radii of these large discs are not particularly accurate.

As the annealing period increases, there are two changes that manifest themselves in the SANS data: (1) there is an increase in intensity, I (not shown in Fig. 1 due to the rescaling of the data); and (2) a shift of the broad peak (i.e., fingerprint for interacting objects), when present, to lower q values (indicated by the arrow in Fig. 1(a). The increase of the low-q intensity is related to an increase of the average bicelle size, which can be determined by fitting the data with the CSD model (solid lines in Fig 1), while a shift in the peak position toward low q indicates an increased interparticle distance between discs. Since the CSD model assumes monodisperse discs, the good agreement between the data and the best fits implies that at any given time, the growth of nanodiscs is reasonably uniform, supporting the notion that the discs grow by fusing with each other. This initial uniformity of nanodiscs in size is not well yet understood, but indicates a preferred size of the discs at high C_{lp} (i.e., energetically instead of entropically driven). In the case of the [NaCl] = 3 mM at 23 °C sample [Fig. 1(b) and (d)], weak oscillations are observed in the SANS data when the sample is annealed for periods >1 h, a feature presumably related to the onset of the nanodisc-to-ULV transition, making it difficult to fit the data with the CSD model.

For the most part, nanodisc growth is observed in all samples and at all temperatures studied. Average nanodisc radii, $\langle R_d \rangle$ as a function of annealing time for the samples at different temperatures are shown in Fig. 2. Several interesting observations are noted: (1) the initial size (i.e., ~20 min after increasing the temperature from 4 °C) of the nanodiscs is larger in lower C_{lp} (i.e., 0.3 wt.%) samples at a given T_{anneal}; and (2) in the case of same C_{lp} samples, the initial nanodisc size is larger in the higher T_{anneal} samples, implying that within the first 15–20 min nanodiscs grow quickly at an elevated T_{anneal}. These observations demonstrate the instability of nanodiscs both upon dilution and increasing T_{anneal}. It is known that DHPC has a higher solubility (in the form of free monomers) than DMPC, and dilution effectively lowers the concentration of the free monomers in solution, extracting DHPC from the nanodiscs. However, the system is expected to reach a new equilibrium after >10 h at 4 °C. The nanodiscs continue to grow over a period of several hours at a given T_{anneal}. This growth is also due to the continuous depletion of DHPC from the disc's rim. In both cases, the growth rate is believed to be dictated by the degree of deficiency of the rim DHPC. Under this DHPC depleted condition the discs coalesce as soon as they collide with each other. Further depletion of DHPC may lead to the micelle → vesicle transition, which has also been observed in cationic and anionic surfactants mixtures, with micelle → vesicle transition rates on the order of ms [34,35]. It should be pointed out, however, that it is not clear whether or not the growth mechanisms are the same for the different systems.

To evaluate the bicelle growth rate, the planar area (i.e., $2\pi\langle R_d \rangle^2$) of bicelles is plotted as a function of annealing time for the different conditions (Fig. 2). Fig. 2(a) and (b) indicate that the bicelle *growth rate* (slope) at 17 and 23 °C is dictated more by T_{anneal} than C_{lp}—although the final sizes of the discs differ at different C_{lp}. Nevertheless, at a T_{anneal} of 10 °C, the growth rates are remarkably different between the 0.3 and 1.0 wt.% samples [Fig. 2(c) and (d), respectively], namely the 0.3 wt.% nanodiscs grow significantly faster.

In the presence of NaCl, the structure factor accounting for Coulombic interparticle interactions is negligible, and can thus be set approximated to 1. With regard to the salt effect, a significant increase is found in the disc radii from 0 to 3 mM, as a result of charge screening. Nanodisc growth rate also increases at a given C_{lp}. It should be noted that the T_{anneal} = 23 °C SANS curves (Fig. 1) do not plateau in the low q region, implying the presence of large discs, resulting in large uncertainties regarding the radii of nanodiscs at this temperature. The Debye screening length, κ^{-1} of a solution containing a monovalent salt can be estimated as $\frac{3.04}{\sqrt{S}}$ Å [36,37], where S is the molarity of the salt, yielding a κ^{-1} of 56 Å and >270 Å for the mixtures of 3 and 0 mM [NaCl], respectively—assuming the complete dissociation of Na^+ from DMPG. The increased size and growth rate are presumably the result of a higher collision frequency between nanodics, because of the small κ^{-1}.

3.1.1. DLVO theory model

In this section, normalized DLVO potentials [27,28] are used to understand nanodisc growth based on the method developed by Sabín et al. for liposomes of similar size [38]. Although the very initial growth of nanodiscs was not attainable (<20 min at T_{anneal}), the first measured SANS data will be used to determine the nominal initial disc size. The stability ratio, W is defined as the ratio of growth rate constants in the rapid regime (k_r), implying that almost all collisions between particles lead to the formation of larger particles, and in the slow regime (k_s) the implication is that collisions are only partially effective. Because the system is composed of particles of similar size W is expressed as [28]:

$$W = k_r/k_s \tag{2}$$

A larger W value indicates higher aggregate stability, and vice versa. The rate constant of higher ionic strength (i.e., [NaCl] = 3 mM) samples is assumed to be k_r (i.e., W = 1), since the growth rate of nanodiscs did not increase in the case of [NaCl] = 6 mM

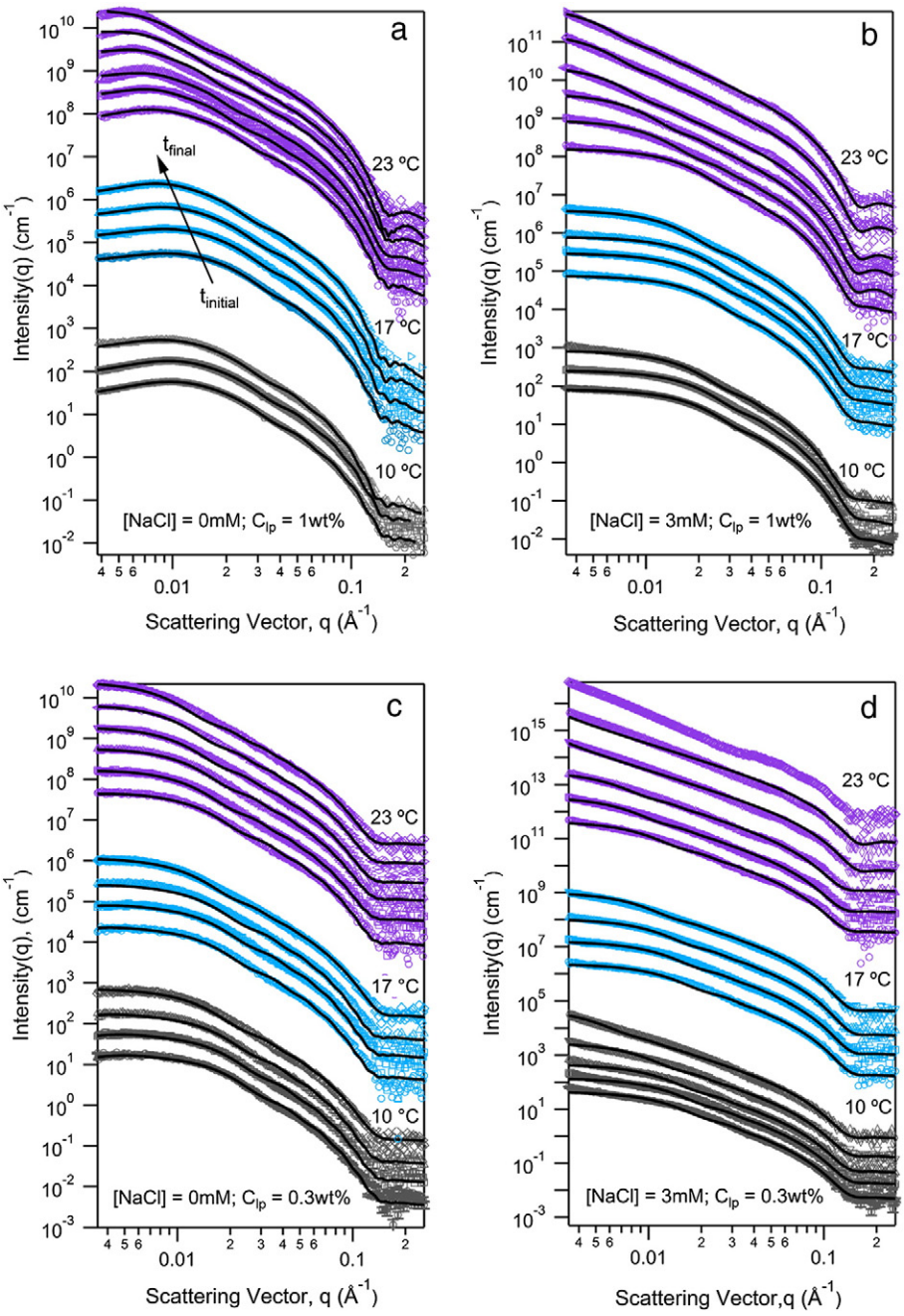

Fig. 1. SANS data and best-fits to the data (solid lines) at 10 °C (grey), 17 °C (blue) and 23 °C (purple) for: (a) [NaCl] = 0 M; C_{lp} = 1 wt.%; (b) [NaCl] = 3 mM or 1 wt.%; (c) [NaCl] = 0 M; C_{lp} = 0.3 wt%; and (d) [NaCl] = 3 mM and C_{lp} = 0.3 wt.%. SANS data were collected at different times, from $t_{initial}$ to t_{final}. The CSD model was used to fit the data. Changes in the SANS data represent changes in bicelle size. Data was gathered over a period of 4 h for T_{anneal} = 17 °C and 23 °C, and over a period of 24 h for the slower growth at T_{anneal} = 10 ° C. The SANS data (in the y-direction) are shifted vertically by arbitrary factors for better viewing the data.

(data not shown). Another approximation is to assume that the interactions between nanodiscs are the same as those between spherical particles. Although geometry is an important determinant of attractive and repulsive energy between particles, the equations are applicable to non-spherical open ULV clusters [39] and therefore should give a satisfactory approximation for disc-shaped bicelles. As a result, the total interaction energy, E between two nanodiscs is approximated as the sum of the van der Waals attractive energy, V_A and the double-layer repulsion energy, V_R of two polyion spheres as follows:

$$E(x) = V_A(x) + V_R(x) \tag{3}$$

The attractive energy as derived by Hamaker can be expressed in the form of Eq. (4) [27,28], while the repulsive energy is expressed by Eq. (5) as follows [40]:

$$V_A(x) = \frac{Aa}{12}\left(\frac{1}{x+2d} - \frac{2}{x+d} + \frac{1}{d}\right) + \frac{A}{6}\ln\left[\frac{x(x+2d)}{(x+d)^2}\right] \tag{4}$$

$$V_R(x) = 2\pi\varepsilon_0\varepsilon_r(a+\Delta)\psi^2\exp[-\kappa(x-2\Delta)], \tag{5}$$

where A is the Hamaker constant, a is the nanodisc mean radius and used as described in [38], x is the surface-to-surface distance between bicelles, d is the double-layer thickness, ε_0 is the vacuum permittivity, ε_r is the relative permittivity of the media, Δ is the Stern layer thickness [taken as the radius of a hydrated sodium ion (Δ = 7.9 Å)], ψ is

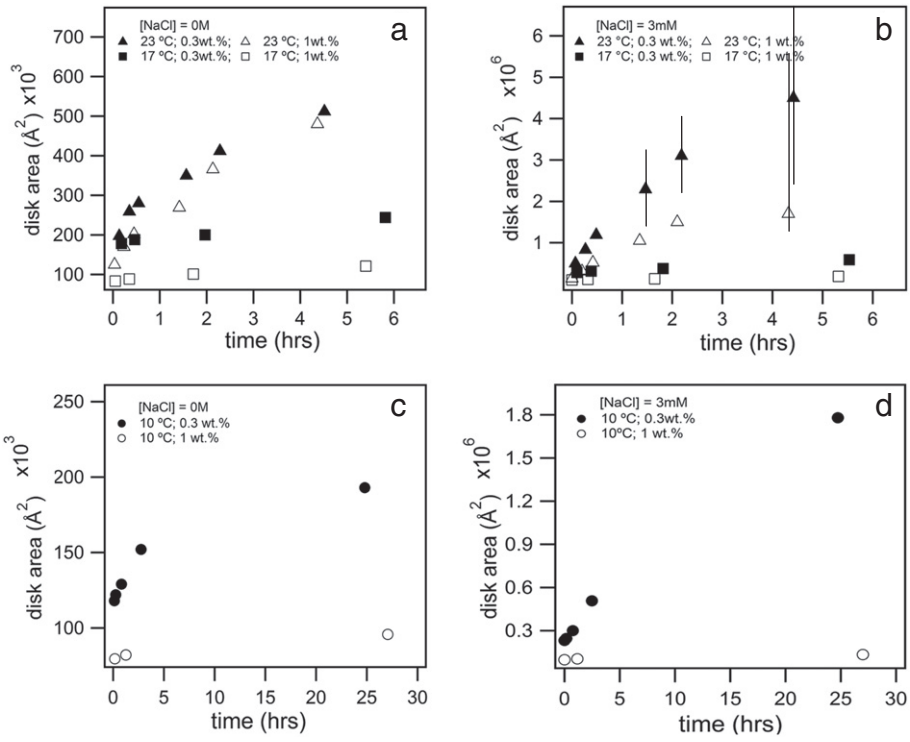

Fig. 2. Average bicellar radii (obtained from best-fits to the data shown in Fig. 1 using the CSD model) as a function of time for the following conditions: (a) [NaCl] = 0 mM at T_{anneal} = 17 and 23 °C; (b) [NaCl] = 3 mM at T_{anneal} = 17 and 23 °C. At 10 °C samples were monitored over an extended period of time due to the slower growth kinetics in the case of both (c) 0 and (d) 3 mM [NaCl] mixtures. The error bars are either smaller than the size of the symbols or as otherwise shown.

the surface potential and is approximated by the Zeta potential ζ, and κ is the reciprocal Debye length.

W is used in a semi-empirical fashion to determine A by adjusting it, in order to minimize its associated errors, as follows:

$$W = \frac{\int_0^\infty \frac{\beta(u)}{(u+2a)^2} \exp\frac{E}{k_bT} du}{\int_0^\infty \frac{\beta(u)}{(u+2a)^2} \exp\frac{V_A}{k_bT} du} \tag{6}$$

$$\beta(u) = \frac{6u^2 + 13u + 2a^2}{6u^2 + 4ua} \tag{7}$$

$$u = \frac{x - 2a}{a}, \tag{8}$$

where k_b is the Boltzmann constant and T is the absolute temperature. Once the Hamaker constants were determined, the DLVO attractive energy, E was calculated using Eqs. (3)–(5), including the initial values for all variables. E was then normalized by dividing by k_bT.

Table 1 shows the growth rates, measured ζ, calculated A and DLVO potentials at the Stern layer. The trend of ζ increasing with increased salt concentration has been reported in liposomal systems at low ionic strengths [41]. The calculated values of A (1×10^{-19} J to 5×10^{-19} J) are higher than reported by Sabin et al. for liposomes (1×10^{-21} J to 7×10^{-20} J) [41], but lower than the values reported by Ahmed and Jones for the liposomes used in their study (up to 7×10^{-18} J) [42]. Growth rate is also found to be positively correlated with the absolute DLVO potentials at the Stern layer, which indicates attraction (negative) between nanoparticles, a result consistent with the fact that nanodiscs are observed to grow under all of the conditions studied.

Table 1
Parameters used for model development which resulted in Hamaker constants and DLVO potentials at the Stern layer (Δ = 7.9 Å). The attractive DLO potential at the Stern layer is higher for systems with faster rates of disc growth.

	Initial growth rate Å^2/min	Zeta potential (measured) *mV*	Hamaker Constant, *A* (calculated) J	E/k_bT at Stern layer unitless
T = 10 °C				
1 wt. %; 3 mM	93	2.8	1.82×10^{-19}	−22.7
0.3 wt.%; 3 mM	1.4×10^3	2.7	3.96×10^{-19}	−70.0
1 wt.%; 0 mM	39	2.5	1.36×10^{-19}	−15.8
0.3 wt.%; 0 mM	3.2×10^2	2.3	2.55×10^{-19}	−34.4
T = 17 °C				
1 wt.%; 3 mM	7.2×10^2	2.8	2.21×10^{-19}	−27.3
0.3 wt.%; 3 mM	2.0×10^3	2.7	2.96×10^{-19}	−55.2
1 wt.%; 0 mM	2.8×10^2	2.5	1.24×10^{-19}	−14.3
0.3 wt.%; 0 mM	6.1×10^2	2.3	1.65×10^{-19}	−25.5
T = 23 °C				
1 wt.%; 3 mM	1.4×10^4	2.8	4.62×10^{-19}	−63.4
0.3 wt.%; 3 mM	2.7×10^4	2.7	3.77×10^{-19}	−111.0
1 wt.%; 0 mM	3.8×10^3	2.5	2.08×10^{-19}	−27.4
0.3 wt.%; 0 mM	4.7×10^3	2.3	2.00×10^{-19}	−31.6

Fig. 3 shows the calculated DLVO potential as a function of x at T_{anneal} = 10, 17 and 23 °C. In each case, attractive forces dominate because of the low ζ. As shown in the insets to Fig. 3, there is a strong linear correlation between the growth rate of nanodiscs and the DLVO potential at the Stern layer. Linear fits to the data extrapolate to a zero growth rate at an attractive DLVO potential. However, zero growth should only occur when the repulsive DLVO potential exceeds the thermal energy (k_bT). This could be attributed to two possible reasons: (1) the aforementioned linear relationship may break down at extremely low DLVO potentials; and (2) the fact that the interparticle potential is not the only factor dictating disc coalescence, further confirms the notion that the quantity of DHPC present at the nanodisc's rim plays an important role in its growth mechanism.

At all temperatures, disc growth rate is fastest for the C_{lp} = 0.3 wt.% with 3 mM [NaCl] sample. One reason for this is the lower attractive energy, V_A, as well as a rapid exponential decrease in the repulsive energy, V_R with distance, i.e., increased ionic strength results in a decreased Debye length, consistent with the lower E value (Table 1). In addition, ζ is larger at high C_{lp} (i.e., 1.0 wt.%) at corresponding salinities, presumably leading to an increase in V_R, and thus a diminished rate of

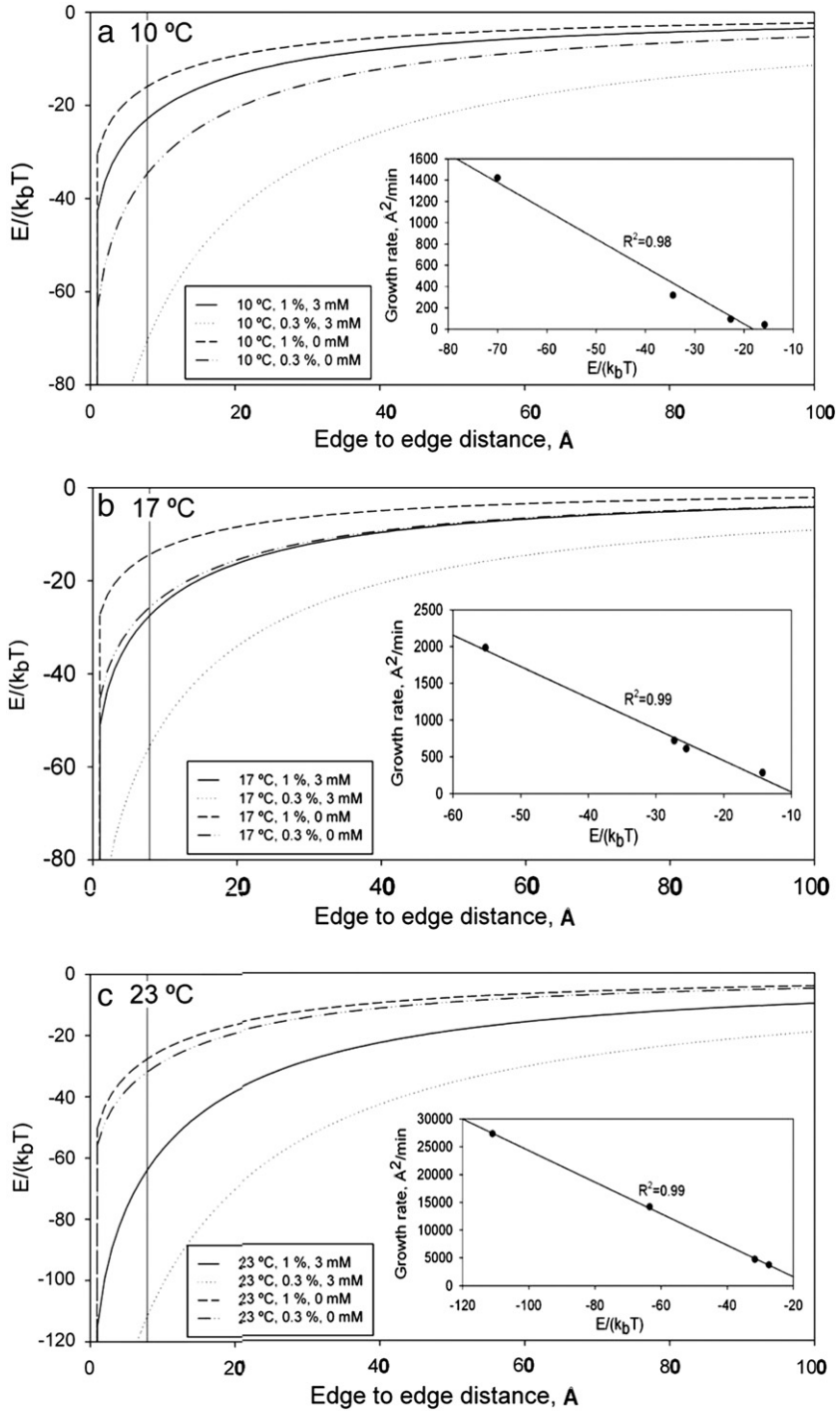

Fig. 3. DLVO potentials, E/(k_bT), as a function of disc separation at (a) 10 °C, (b) 17 °C and (c) 23 °C. The Stern layer thickness is 7.9 Å and is marked with a solid vertical line. Inserts to the figures show that nominal initial growth rate, measured by SANS, correlates well with DLVO potential calculated at the Stern layer thickness.

growth. The overall lower content of DHPC in $C_{lp}=0.3$ wt.% samples also induces instability in the nanodiscs. However, for all temperatures the opposite can be said for the $C_{lp}=1$ wt.% sample with no salt.

3.1.2. Temperature dependence

The most common approach for studying the temperature dependence of chemical reactions is the use of the Arrhenius equation, where the natural logarithm of the rate constant and the reciprocal absolute temperature are linearly related, as shown in Eq. (9):

$$k = k_0 \exp(-Q/k_b T), \tag{9}$$

where Q is the activation energy and k_0 is the upper-limit rate prefactor. Fig. 4 shows the temperature dependence of the rate constant obtained from the initial linear portion of the disc growth curve. The result indicates an Arrhenius-like temperature dependence in the case of the 1 wt.% sample, while a strong deviation is found in the 0.3 wt% sample data, implying that other temperature dependent mechanisms are involved.

The trend observed indicates that the disc growth rate increases significantly with increased thermal energy. However, important information can be revealed through further analysis of the contributions from k_0 and Q as a function of C_{lp} and salinity. Table 2 illustrates the calculated k_0 and Q from Eq. (9). The fact that k_0 is higher in the case of 1 wt.% and 3 mM [NaCl] samples implies an overall higher disc collision frequency, presumably due to a combination of a higher number density ($C_{lp}=$ 1 wt.%) and a smaller Debye length ([NaCl] = 3 mM). The obtained activation energy, Q is similar to the average thermal energy ranging from 2.0 kJ/mol to 3.9 kJ/mol over the temperatures studied. In comparison with the initial attractive energy between discs at the Stern layer thickness calculated using DLVO theory—above 15 k_bT (Table 1), this result is consistent with the observed initial fast growth of the discs. Moreover, the fact that the Q value for 1 wt.% samples is higher than that for 0.3 wt.% samples, implies that nanodisc stability is greater when more of the short-chain lipid (i.e., DHPC) is present within the disc.

3.2. Self-folding of nanodiscs

After a prolonged period of temperature annealing (i.e., 10, 17 and 23 °C) of the individual samples, all samples were heated to 50 °C (T_{50}) so that SANS measurements could be conducted to determine the relationship between the final size of the nanodiscs and that of the end-state ULVs. Fig. 5 shows that the scattering data of the T_{50} samples resemble those of ULVs shown in previous reports [7,11,19]. Moreover, these data can be best fit using the PV model (see experimental procedure section). The intensity oscillations observed along the curves and their positions, reveal ULV polydispersity and their average size, respectively. Peak widths become broader with increased temperature, indicating an increase in ULV polydispersity, p. It should also be noted that SANS data obtained from [NaCl] = 3 mM samples, which were annealed at $T_{anneal}=23$ °C (T_M of DMPC) show neither low-q plateaus nor well-defined oscillations, resulting in best fits with larger uncertainties, and where only the smallest possible average vesicle radius $\langle R_v \rangle$ is determined. This result can be rationalized by the fact that the miscibility between DMPC and DHPC increases dramatically (both lipids are now in the L_α phase), causing DHPC to migrate away from the disc rim, resulting in unstable nanodiscs due to the exposure of the hydrophobic region to the aqueous phase. This instability manifests itself in discs continuously coalescing throughout the annealing process which lasted more than 5 h. Hence, even before the temperature was increased to 50 °C, nanodiscs are present in a range of sizes, and some had even self-folded into ULVs. This hypothesis is consistent with the wide range of ULV sizes observed. Fig. 5 shows SANS data of samples incubated at T_{50} for 4 h, while Fig. 6(a) and (b) shows the average vesicle radii, $\langle R_v \rangle$ and p of the end-state ULVs, respectively, obtained from the best fits to the SANS data shown in Fig. 5.

Table 2
Summary of k_0 and Q for disc growth under all conditions.

C_{lp} (wt.%)	[NaCl] (mM)	k_0 (Å^2/min)	Q (kJ/mol)
0.3	0	3.97×10^{28}	2.05
0.3	3	1.66×10^{31}	2.21
1	0	1.88×10^{46}	3.51
1	3	1.40×10^{51}	3.86

3.2.1. Effects of C_{lp} and salinity

In the absence of NaCl $\langle R_v \rangle$ varies from approximately 100 Å to 200 Å as C_{lp} changes from 0.3 to 1 wt.%, a result that is practically independent of T_{anneal} [Fig. 6(a)]. This is consistent with the C_{lp} dependence reported by several previous studies [7,11]. Nevertheless, this trend in $\langle R_v \rangle$ is not expected. Since the terminal size of nanodiscs is always smaller for higher C_{lp} (i.e., 1 wt.%) samples at all T_{anneal} (i.e., 10, 17 and 23 °C), we expected ULVs to follow the same trend if the discs were to self-fold immediately after being heated to 50 °C. The current discrepancy between the trend in $\langle R_v \rangle$ and that in the final $\langle R_d \rangle$ indicates that fast disc coalescence (in 1 wt.% samples) may take place during the slow increase of sample temperature in the 50 °C oven—this will be discussed further in the following section.

With regard to the effect of salinity, $\langle R_v \rangle$ increases at least by 50% (from ~100 Å to ~150 Å) for the $C_{lp}=0.3$ wt.% sample and by 75% (from ~200 Å to ~350 Å) for the $C_{lp}=1$ wt.% sample when the salt

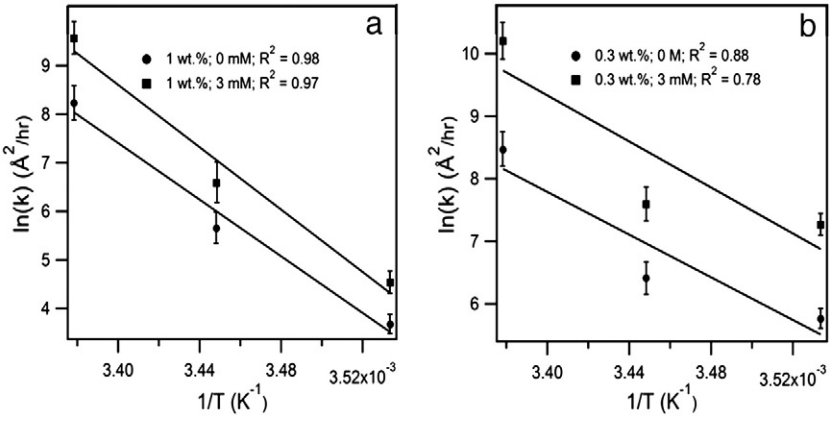

Fig. 4. T dependence of disc growth rate (k) for: (a) 1 wt.% and (b) 0.3 wt.% at [NaCl] = 0 M (circles) and 3 mM (squares).

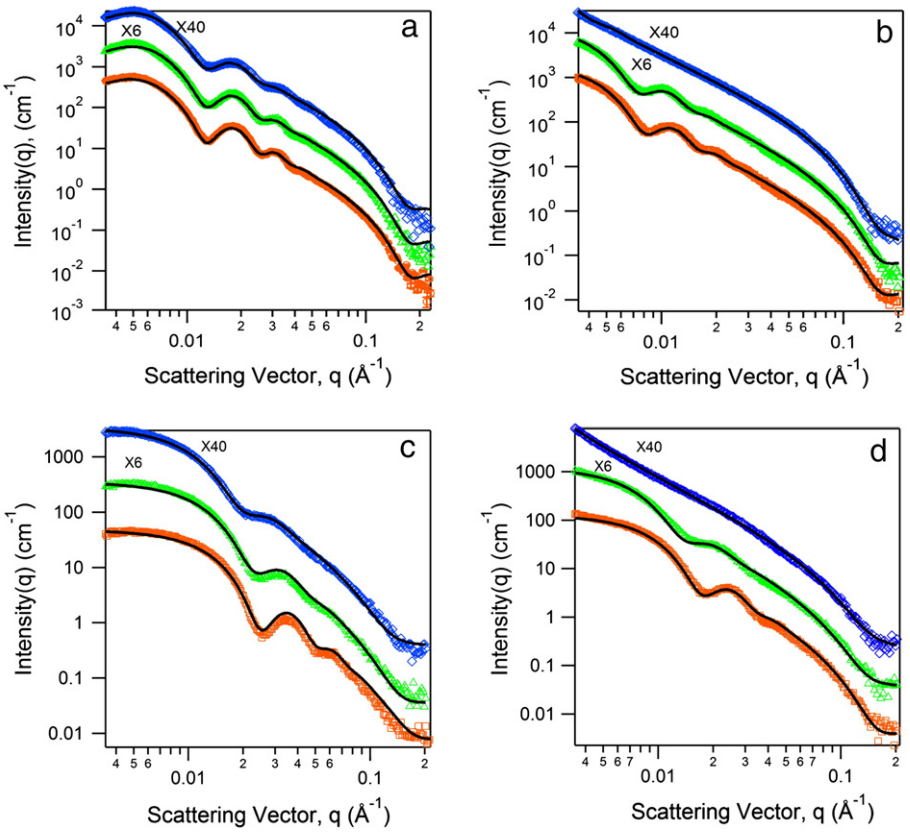

Fig. 5. SANS data and best-fits to the data (solid lines) of samples incubated at 50 °C for 4 h. (a) [NaCl] = 0 M; C_{lp} = 1 wt%; (b) [NaCl] = 3 mM; C_{lp} = 1 wt%; (c) [NaCl] = 0; C_{lp} = 0.3 wt%; (d) [NaCl] = 3 mM; C_{lp} = 0.3 wt%. The samples were annealed at T_{anneal} = 10 (orange squares), 17 (green triangles) and 23 °C (blue diamonds), respectively, prior to being heated to 50 °C. Intensities are scaled to allow for better viewing of the data.

concentration goes from 0 to 3 mM [Fig. 6(a)] at T_{anneal} = 10 and 17 °C. The observation of a larger $\langle R_v \rangle$ with increased salt content is a result of charge screening, which enhances the collision frequency of nanodiscs, consistent with previous reports [25,43,44]. In the case of 23 °C samples, $\langle R_v \rangle$ values in the case of [NaCl] = 3 mM are estimated to be on the low side, due to the high uncertainty associated with the best fit results (as mentioned previously), and are always larger than those of the samples in the absence of NaCl. ULV polydispersity, p decreases with increased C_{lp} implying that more uniform size ULVs are obtained at a higher C_{lp}, a result that is currently not well understood. Moreover, p increases with increased salinity, presumably due to an increased frequency of "effective collisions" which result in "entropy-driven size" ULVs with greater polydispersities.

3.2.2. Effect of T_{anneal}

For both lipid concentration samples (C_{lp} = 0.3 wt.% and 1 wt.%) studied in the absence of NaCl, $\langle R_v \rangle$ remains constant at the different T_{anneal} (i.e., 10, 17 and 23 °C). The fact that thermal history does not affect the final ULV size *seems* to be inconsistent with a previous report, where $\langle R_v \rangle$, at a given C_{lp}, was found to be larger through a slow temperature annealing process, where nanodiscs persisted over longer periods of time at higher temperature [25]. As mentioned in a previous section, this unexpected result is likely attributed to the following kinetics: (1) the disc coalescence rate, r_c; (2) the self-folding rate, r_{s-f}; and (3) the rate of increasing temperature, r_T. The fact that the first attainable $\langle R_d \rangle$ data points for 1.0 wt.% samples are 108 Å [Fig. 2 (c)] and 135 Å [Fig. 2(a)] at T_{anneal} = 10 and 23 °C,

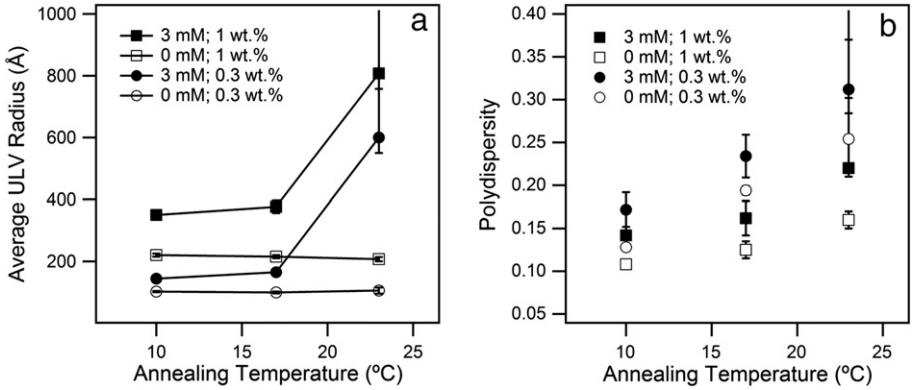

Fig. 6. (a) Average ULV radii $\langle R_v \rangle$ and polydispersities, p obtained from the best-fits to the data (50 °C) in Fig. 5. C_{lp} = 1 wt% (squares) at [NaCl] = 0 (open) and [NaCl] = 3 mM (filled) and C_{lp} = 0.3 wt.% (circles) at [NaCl] = 0 (open) and [NaCl] = 3 mM (filled). The error bars are either smaller than the size of the symbols or as otherwise shown.

respectively indicates that the system responds quickly to changes in temperature. Although the disc growth rate slows down with time, it is still present after the initial rapid growth period. For example, it takes hours for discs annealed at 17 °C to increase by 30% in radius [Fig. 2(a)], while such a change takes only minutes in samples annealed at 23 °C. Hence, it is evident that the "effective collision" rate increases dramatically with increased temperature, presumably driven by the rim DHPC migrating into the DMPC bilayer, promoting disc coalescence. Another kinetically controlling mechanism—self-folding—described by r_{s-f} is dictated by disc stability associated with reduced membrane rigidity and an insufficient amount of rim DHPC. In other words, a faster r_{s-f} is anticipated for lower C_{lp} samples at a higher T_{anneal}. Finally, the experimental r_T can strongly affect r_{s-f} resulting in a range of ULV sizes.

Fig. 7 schematically describes the growth of nanodiscs prior to ULV formation. The initial fast growth regime has two contributing factors: dilution (from 20 wt.% to the final C_{lp}) and increase in temperature (from 4 °C to T_{anneal}). The former leads to the loss of DHPC to the water phase, while the latter enhances the miscibility between DMPC and DHPC. Both mechanisms effectively drive DHPC away from the rim of the discs.

As the samples are annealing at 10, 17 or 23 °C, the discs continue to grow at a slower rate, which is higher (i.e., a greater slope in Fig. 7) at a higher T_{anneal}. However, in the case of the lower T_{anneal} (e.g., 10 °C) sample, after it was heated to 50 °C the discs coalesced at such a rate that they eventually caught up to those of the high-T_{anneal} (e.g., 23 °C) sample if r_{s-f} is slow enough. The same principle applies to the lower C_{lp} samples (0.3 wt.%), except that in their case r_{s-f} is much faster (due to the smaller total amount of DHPC in the mixture) and a lower collision frequency (due to lower number density of discs), resulting in a smaller $\langle R_v \rangle$. The proposed scheme implies that r_{s-f} has to be fast enough in order to observe a meaningful correlation between final $\langle R_d \rangle$ and $\langle R_v \rangle$, which presumably can be achieved by increasing the molar ratio of the long- to short- chain lipids, decreasing the T_M of the long-chain lipid, and reducing C_{lp}.

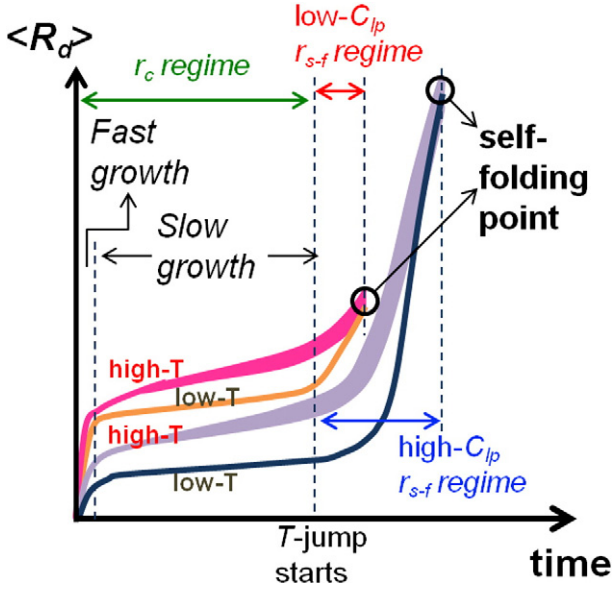

Fig. 7. Proposed growth kinetics of nanodiscs as a function of time in cases of low-C_{lp} (magenta and orange) and high-C_{lp} (light purple and dark blue) at high (bold curves) and low (narrow curves) T_{anneal}. $\langle R_d \rangle$ increases fast initially, then slowly in the later annealing regime. A wider size distribution of disc radii (bolder curves) at higher T_{anneal} is expected due to entropy-driven coalescence. The earlier self-folding of low-C_{lp} nanodiscs, compared to those at high-C_{lp}, can be attributed to insufficient amounts of DHPC at the disc's rim due to the loss of DHPC to solution.

Polydispersity also increases with increasing T_{anneal} [Fig. 6(b)]. This result is anticipated because the final size distribution of nanodiscs is broader at higher T_{anneal} due to the formation of larger, entropy-driven coalescing discs (Fig. 7). Although the current CSD model provides reasonable best fitting results without the consideration of polydispersity, the ULVs do however inherit the polydispersity of their nanodisc precursors. The same can be said for samples in the presence of NaCl, where both $\langle R_v \rangle$ and p increase with increasing T_{anneal}, consistent with one of our previously published results [25].

3.2.3. Role of precursor bicelles in ULV formation

Since DMPC and DHPC have the same phosphatidylcholine headgroup, to a first approximation the total surface area of a nanodisc should be proportional to the number of molecules within it. From the best fits, the average nanodisc radius, $\langle R_d \rangle$ and shell thickness, t_{shell}, the planar nanodisc surface area, which is presumably composed of DMPC and DMPG mostly, is calculated as $A_{disc} = 2\pi\,(\langle R_d \rangle + t_{shell}/2)^2$. This average surface area of the final size discs measured for each sample at each T_{anneal} is then compared to the average surface area of the corresponding vesicle, which is calculated as $A_{vesicle} = 4\pi\,[\langle R_o \rangle^2 + \langle R_i \rangle^2]$). The ratio of $A_{vesicle}$ to A_{disc} provides an estimate of the aggregation number of final-sized discs to ULVs, as listed in Table 3. As mentioned previously, the smaller nanodiscs observed in the higher C_{lp} (i.e., 1 wt.%) samples result in larger end-state ULVs than those of the lower C_{lp} (0.3 wt.%) samples. Disc aggregation numbers to form one ULV are found in the range from >2 to 20. Interestingly, in the case of 0.3 wt.% samples, nanodisc growth practically ceases after the annealing period and prior to self-folding. In one occasion (T_{anneal} = 23 °C and [NaCl] = 0 mM), $A_{vesicle}/A_{disc}$ results in a value of 0.66, implying that the planar region of the nanodiscs might contain a significant amount of DHPC, while ULVs are mostly composed of DMPC and DMPG.

3.2.4. Reaction limited coalescence

Since the DHPC at the disc's rim stabilizes the nanodisc morphology, it is presumed that only edge-to-edge collisions result in the discs coalescing with each other (Fig. 8). This process continues until the nanodiscs eventually become unstable and fold into ULVs. Nevertheless, it should be pointed out that not all edge-to-edge collisions are effective collisions. Generally speaking, the aggregation of colloids can be classified into two regimes: diffusion limited colloid aggregation (DLCA), and reaction limited colloid aggregation (RLCA) [45]. DLCA describes the cases where aggregation occurs immediately upon contact, in other words, all collisions are effective. Thus its aggregation rate is limited by the frequency of the collisions due to diffusion. In the case of RLCA, the aggregation rate mainly depends on the frequency of effective collisions [45–47].

Table 3
The average surface area of nanodiscs at the end of the annealing process and the average surface area of vesicles formed after heating to 50 °C. The number of discs necessary to form a single vesicle is given by $A_{vesicle}/A_{disc}$.

[NaCl]; C_{lp}	T_{jump} (°C)	Disc surface area (Å^2)	Vesicle surface area (Å^2)	$A_{vesicle}/A_{disc}$
0 mM; 1 wt.%	10–50	$(1.29 \pm 0.05) \times 10^5$	$(1.42 \pm 0.10) \times 10^6$	11.0
	17–50	$(1.57 \pm 0.06) \times 10^5$	$(1.37 \pm 0.13) \times 10^6$	8.68
	23–50	$(5.33 \pm 0.08) \times 10^5$	$(1.27 \pm 0.15) \times 10^6$	2.39
3 mM; 1 wt.%	10–50	$(1.72 \pm 0.06) \times 10^5$	$(3.41 \pm 0.1) \times 10^6$	19.8
	17–50	$(2.33 \pm 0.09) \times 10^5$	$(3.91 \pm 0.2) \times 10^6$	16.8
	23–50	$> 1.83 \times 10^6$	$> 1.71 \times 10^7$	–
0 mM; 0.3 wt.%	10–50	$(2.46 \pm 0.06) \times 10^5$	$(3.69 \pm 0.10) \times 10^5$	1.49
	17–50	$(2.88 \pm 0.09) \times 10^5$	$(3.54 \pm 0.09) \times 10^5$	1.22
	23–50	$(5.0 \pm 0.1) \times 10^5$	$(3.90 \pm 0.09) \times 10^5$	0.66
3 mM; 0.3 wt.%	10–50	$(1.30 \pm 0.06) \times 10^6$	$(6.67 \pm 0.06) \times 10^5$	0.51
	17–50	$(6.8 \pm 0.1) \times 10^5$	$(8.47 \pm 0.20) \times 10^5$	1.24
	23–50	$> 2.44 \times 10^6$	$> 9.59 \times 10^6$	–

Several indicators can be used to determine whether the system of interest falls either in the DLCA or RLCA category. In this case, a high activation energy, Q determined from the Arrhenius kinetics and a high stability ratio, W imply that only a small fraction of collisions is effective, evidence supporting the RLCA regime. Although the required edge-to-edge collision may play a role in lowering the effective collision rate, it does not explain, however, why the higher coalescence rate is observed in lower C_{lp} samples—presumably attributed to unstable nanodiscs.

Another piece of evidence for the presence of unstable nanodiscs in low C_{lp} samples, compared to high C_{lp} samples, is the small value of $A_{vesicles}/A_{disc}$ (Table 3), indicating rapid self-folding and the formation of ULVs. Similar results have been reported in DMPC/bile salt mixtures, where increased dilutions (i.e., lower C_{lp} samples) of nanodiscs resulted in smaller radii ULVs [18,48].

3.2.5. Applicability of DLVO model

The current application of DLVO theory is based on the observed growth rate of nanodiscs. This approach is only valid when the ratio of effective-to-actual collisions is practically invariant. However, in the present case effective collisions are dictated by the availability of the edge-stabilizer, DHPC, at the disc's rim, which happens to continuously vary as disc coalesce. This mechanism has been proposed in literatures in light of theory [15] and experimental results [12,25]. Future SANS measurements on mixtures of deuterated DMPC and hydrogenated DHPC under a contrast-matched condition should be able to verify this scenario. The equations describing the DLVO model were derived based on the assumption of spherical aggregates [38], where effective collisions are assumed to be isotropic. In the case of nanodiscs, effective collisions are only expected to take place during edge-to-edge collisions, which are of lower probability than isotropic collisions.

Fractal models have been used to describe agglomeration, and it was conlculded that $R_g(t) \propto t^{1/d_f}$, where R_g is the radius of gyration and d_f is the fractal dimension of the resulting structure, obtained from the decay slope of high-q scattering data. [45,46]. Lin et al. described colloid agglomeration with diffusion and reaction limited models, corresponding to $W = 1$ and $W \gg 1$ having fractal dimensions of 1.8 and 2.1, respectively [46]. It should be noted that the current system does not resemble a conventional DLCA or RLCA process for two reasons. First, there is no coalescence (fusion) involved in regular colloidal systems—resulting in a final morphology of a fractal dimension. However, the coalescence plays a crucial role in the DMPC/DHPC/DMPG mixture in order to stabilize the nanodiscs. Second, unlike the system in the study, the aggregation of colloidal particles continues with time in a typical RLCA and DLCA process. Therefore, the analysis of fractal dimensions is not applicable in this study.

4. Conclusion

We report on the growth of nanodiscs in dilute lipid mixtures using time-resolved SANS. The study was conducted as a function of C_{lp} (0.3 and 1.0 wt.%), salinity ([NaCl] = 0 and 3 mM) and T_{anneal} (10, 17 and 23 °C). We have determined that the aggregation of these nanoparticles is well-described by a non-fractal reaction limited colloid aggregation (RLCA) coalescence. Nanodiscs of the current charge density ([DMPG]/[DMPC] = 0.01) continuously increase in size at lower temperatures, implying that they are inherently metastable structures. This observation, although not new [26], has never been analyzed in the detail that we have reported here. The growth of nanodiscs upon dilution (from 20 wt.% to 1 wt.% or 0.3 wt.%) and/or annealing temperature of 10, 17 or 23 °C (prior to self-folding) can be described as taking place in two stages, i.e., fast and slow growth regimes. Analysis by DLVO theory, based on the slow growth rate (as measured by SANS), provides a way to better understand the interaction of nanodiscs. However, DLVO theory does not account for the C_{lp}-dependent instability of the discs, which presumably results from insufficient amounts of the rim stabilizer, DHPC. An Arrhenius kinetic model is also applied to study the activation energy of the disc coalescence. Although a non-linear relationship between $\ln(k)$ and $1/T$ is found, the facts that the upper-limit k (i.e., k_0) increases with C_{lp}, and that the activation energy Q decreases with C_{lp}, all agree reasonably well with the physical insights that we have gained of this system through experiments described here.

Generally speaking, the observed growth rate of the nanodiscs shows stronger temperature dependence than those associated with either C_{lp} or salinity (except for samples at 10 °C). The fact that a T-jump (from T_{anneal} to 50 °C) experiment shows only a marginal dependence of $\langle R_v \rangle$ on $\langle R_d \rangle$, indicates that in the case of high-C_{lp} samples the disc coalescence rate is extremely fast upon increasing T, while disc coalescence is limited for low-C_{lp} samples. This is rationalized by the presence of less stable nanodiscs, which self-fold much faster in the case of lower C_{lp} samples due to insufficient amounts of DHPC (migrating to the bilayered planar region) as temperature increases, prohibiting the nanodiscs from growing further. This study not only provides confirmation of an earlier hypothesis regarding the growth of nanodiscs and the eventual formation of self-assembled ULVs, but also lends insight in ways to design and control the size of spontaneously forming nanodiscs or vesicles for possible future applications. However, because of the extended data collection times required by SANS, the immediate increase of $\langle R_d \rangle$ upon dilution was not accessible. Future work will focus on the very early growth mechanism of nanodiscs using dynamic light scattering and SAXS at synchrotron sources.

Acknowledgement

This work utilizes the Oak Ridge National Laboratory's High Flux Isotope Reactor, which is sponsored by the Scientific User Facilities Division, Office of Basic Energy Sciences, U.S. Department of Energy. M.-P. N. acknowledges the support of startup fund from the Institute of Materials Science (IMS) at the University of Connecticut (UConn), UConn faculty large research grant and NSF grant (CMMI 1131587). D. S. is supported by the NSERC Alexander Graham Bell graduate scholarship. S. M. is funded by the Canadian Institutes of Health Research Training Grant in Vascular Research and Ontario Graduate Scholarship. J.K. is supported by Oak Ridge National Laboratory's (ORNL) Laboratory Directed Research and Development (LDRD) and Program Development programs.

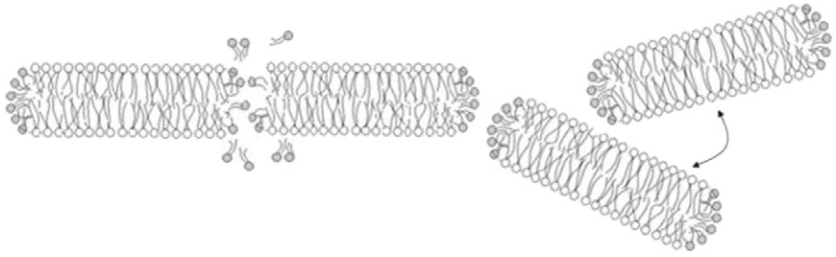

Fig. 8. Effective collision of discs in the edge-to-edge orientation. Loss of DHPC from the disc's edge (gray lipids) contributes to bicelle instability.

Appendix A. Supplementary data

Supplementary data to this article can be found online at http://dx.doi.org/10.1016/j.bbamem.2012.11.002.

References

[1] J.R. Silvius, Solubilization and functional reconstitution of biomembrane components, Annu. Rev. Biophys. Biomol. Struct. 21 (1992) 323–348.
[2] H. De Boeck, R. Zidovetzki, Interactions of saturated diacylglycerols with phosphatidylcholine bilayers: a 2H NMR study, Biochemical 31 (1992) 623–630.
[3] C.R. Sanders II, J.P. Schwonek, Characterization of magnetically orientable bilayers in mixtures of dihexanoylphosphatidylcholine and dimyristoylphosphatidylcholine by solid-state NMR, Biochemistry 31 (1992) 8898–8905.
[4] C.R. Sanders II, G.C. Landis, Reconstitution of membrane proteins into lipid-rich bilayered mixed micelles for NMR studies, Biochemistry 34 (1995) 4030–4040.
[5] C.R. Sanders II, R.S. Prosser, Bicelles: a model membrane system for all seasons? Structure 6 (1998) 1227–1234.
[6] A. Diller, C. Loudet, F. Aussenac, G. Raffard, S. Fournier, M. Laguerre, A. Grélard, S.J. Opella, F. Marassi, E.J. Dufourc, Bicelles: a natural 'molecular goniometer' for structural, dynamical and topological studies of molecules in membranes, Biochemistry 91 (2009) 744–751.
[7] M.-P. Nieh, C.J. Glinka, S. Krueger, R.S. Prosser, J. Katsaras, SANS study of the structural phases of magnetically alignable lanthanide-doped phospholipid mixtures, Langmuir 17 (2001) 2629–2638.
[8] M.-P. Nieh, V.A. Raghunathan, C.J. Glinka, T.A. Harroun, G. Pabst, J. Katsaras, Magnetically alignable phase of phospholipid "bicelle" mixtures is a chiral nematic made up of wormlike micelles, Langmuir 20 (2004) 7893–7897.
[9] L. van Dam, G. Karlsson, K. Edwards, Direct observation and characterization of DMPC/DHPC aggregates under conditions relevant for biological solution NMR, Biochim. Biophys. Acta Biomembr. 1664 (2004) 241–256.
[10] A. Walter, P.K. Vinson, A. Kaplun, Y. Talmon, Intermediate structures in the cholate-phosphatidylcholine vesicle-micelle transition, Biophys. J. 60 (1991) 1315–1325.
[11] M.-P. Nieh, C.J. Glinka, S. Krueger, R.S. Prosser, J. Katsaras, SANS study on the effect of lanthanide ions and charged lipids on the morphology of phospholipid mixtures, Biophys. J. 82 (2002) 2487–2498.
[12] M.-P. Nieh, N. Kučerka, J. Katsaras, Spontaneously formed unilamellar vesicles, Methods Enzymol. 465 (2009) 3–20.
[13] H. Wu, K. Su, X. Guan, M.E. Sublette, R.E. Stark, Assessing the size, stability, and utility of isotropically tumbling bicelle systems for structural biology, Biochim. Biophys. Acta 1798 (2010) 482–488.
[14] D.D. Lasič, A molecular model for vesicle formation, Biochim. Biophys. Acta Biomembr. 692 (1982) 501–502.
[15] P. Fromherz, C. Röcker, D. Rüppel, From discoid micelles to spherical vesicles: the concept of edge activity, Faraday Spec. Discuss. Chem. Soc. 81 (1986) 39–48.
[16] L.I. Barsukov, Temperature-induced micellar–lamellar transformation in binary mixtures of saturated phosphatidylcholines with sodium cholate, FEBS Lett. 358 (1995) 17–22.
[17] J. Leng, S.U. Egelhaaf, M.E. Cates, Kinetic pathway of spontaneous vesicle formation, Europhys. Lett. 59 (2002) 311–317.
[18] J. Leng, S.U. Egelhaaf, M.E. Cates, Kinetics of the micelle-to-vesicle transition: aqueous lecithin–bile salt mixtures, Biophys. J. 85 (2003) 1624–1646.
[19] M.-P. Nieh, T.A. Harroun, V.A. Raghunathan, C.J. Glinka, J. Katsaras, Concentration independent spontaneously forming biomimetic vesicles, Phys. Rev. Lett. 91 (2003) 158105.
[20] M. Winterhalter, W. Helfrich, Effect of surface charge on the curvature elasticity of membranes, J. Phys. Chem. 92 (1988) 6865–6867.
[21] M.D. Betterton, M.P. Brenner, Electrostatic edge instability of lipid membranes: theoretical study of how charge can form holes on membranes, Phys. Rev. Lett. 82 (1999) 1598–1602.
[22] P.K. Yuet, D. Blankschtein, Molecular-thermodynamic modeling of mixed cationic/anionic vesicles, Langmuir 12 (1996) 3802–3818.
[23] P.K. Yuet, D. Blankschtein, Effect of surfactant tail-length asymmetry on the formation of mixed surfactant vesicles, Langmuir 12 (1996) 3819–3827.
[24] M.-P. Nieh, V.A. Raghunathan, G. Pabst, T.A. Harroun, K. Nagashima, H. Morales, J. Katsaras, P.M. MacDonald, Temperature driven annealing of perforations in bicellar model membranes, Langmuir 27 (2011) 4838–4847.
[25] S. Mahabir, W.K. Wan, J. Katsaras, M.-P. Nieh, The effects of charge density and thermal history on the morphologies of spontaneously formed unilamellar vesicles, J. Phys. Chem. B 114 (2010) 5729–5735.
[26] M.-P. Nieh, P. Dolinar, N. Kučerka, S.R. Kline, L.M. Debeer-Schmitt, K.C. Littrell, J. Katsaras, Formation of kinetically trapped nanoscopic unilamellar vesicles from metastable nanodiscs, Langmuir 27 (2011) 14308–14316.
[27] B.V. Derjaguin, L.D. Landau, Theory of stability of strongly charged lyophobic sols of the adhesion of strongly charged particles in solution electrolytes, Acta Physicochim. U.R.S.S. 14 (1941) 633–652.
[28] E.J.W. Verwey, J.Th.G. Overbeek, Theory of stability of lyophobic colloids, Dover Publications, Mineola, New York, 1999.
[29] S.R. Kline, Reduction and analysis of SANS and USANS data using IGOR Pro, J. Appl. Crystallogr. 39 (2006) 895–900.
[30] J.B. Hayter, J. Penfold, Self-consistent structural and dynamic study of concentrated micelle solutions, J. Chem. Soc., Faraday Trans. 1 77 (1981) 1851–1863.
[31] J.B. Hayter, J. Penfold, An analytic structure factor for maroion solutions, Mol. Phys. 42 (1981) 109–118.
[32] W.C. Hung, F.Y. Chen, Osmotic threshold and water association for phospholipid gel phase bilayers, Chin. J. Phys. 38 (2000) 882–892.
[33] C.W. Meuse, S. Krueger, C.F. Majkrzak, J.A. Dura, J. Fu, J.T. Connor, A. Plant, Hybrid bilayer membranes in air and water: infrared spectroscopy and neutron reflectivity studies, Biophys. J. 74 (1998) 1388–1398.
[34] A.J. O'Connor, T.A. Hatton, A. Bose, Dynamics of micelle-vesicle transitions in aqueous anionic/cationic surfactant mixtures, Langmuir 13 (1997) 6931–6940.
[35] S. Schmolzer, D. Grabner, M. Gradzielski, T. Narayanan, Millisecond-range time-resolved small-angle X-ray scattering studies of micellar transformations, Phys. Rev. Lett. 88 (2002), 258301 1–4.
[36] W.B. Russel, D.A. Saville, W.R. Schowalter, Colloidal Dispersions, Cambridge University Press, Cambridge, 1989.
[37] J. Israelachvili, Intermolecular and Surface Forces, 2nd ed. Academic Press Inc., New York, 1985.
[38] J. Sabín, G. Prieto, P.V. Messina, J.M. Ruso, R. Hidalgo-Alvarez, F. Sarmiento, On the effect of Ca^{2+} and La^{3+} on the colloidal stability of liposomes, Langmuir 21 (2005) 10968–10975.
[39] J. Sabın, G. Prieto, J.M. Ruso, F. Sarmiento, Fractal aggregates induced by liposome–liposome interaction in the presence of Ca^{2+}, EPJE 24 (2007) 201–210.
[40] B. Vincent, H. Bijsterbosch, J. Lyklema, Competitive adsorption of ions and neutral molecules in the stern layer on silver iodide and its effect on colloid stability, J. Colloid Interface Sci. 37 (1970) 171–178.
[41] J. Sabin, G. Prieto, J.M. Ruso, R. Hidalgo-Alvarez, F. Sarmiento, Size and stability of liposomes: a possible role of hydration and osmotic forces, Eur. Phys. J. 20 (2006) 401–408.
[42] K. Ahmed, M.N. Jones, The effect of shear on the desorption of liposomes adsorbed to bacterial biofilms, J. Liposome Res. 13 (2003) 187–197.
[43] B. Yue, C.Y. Huang, M.-P. Nieh, C.J. Glinka, J. Katsaras, Highly stable phospholipid unilamellar vesicles from spontaneous vesiculation: a DLS and SANS study, J. Phys. Chem. B 109 (2005) 609–616.
[44] J. Oberdisse, C. Couve, J. Appell, J.F. Berret, C. Ligoure, G. Porte, Vesicles and onions from charged surfactant bilayers: a neutron scattering study, Langmuir 12 (1996) 1212–1218.
[45] M.Y. Lin, H.M. Lindsay, D.A. Weitz, R.C. Ball, R. Klein, P.J. Meakin, Universality of colloid aggregation, Nature 339 (1989) 360–362.
[46] M.Y. Lin, H.M. Lindsay, D.A. Weitz, R.C. Ball, R. Klein, P.J. Meakin, Universal reaction-limited colloid aggregation, Phys. Rev. A 41 (1990) 2005–2020.
[47] M.Y. Lin, H.M. Lindsay, D.A. Weitz, R.C. Ball, R. Klein, P.J. Meakin, Universal diffusion-limited colloid aggregation, J. Phys. Condens. Matter 2 (1990) 3093–3113.
[48] S.U. Egelhaaf, P. Schurtenberger, Micelle-to-vesicle transition: a time-resolved structural study, Phys. Rev. Lett. 82 (1999) 2804–2808.